Korean Journal of Chemical Engineering (2024) 41:2541–2551
https://doi.org/10.1007/s11814-024-00218-x

ORIGINAL ARTICLE

Mechanochemical Synthesis of Multicomponent Bismuth-Based Molybdate Catalysts for Propylene Ammoxidation to Produce Acrylonitrile

ChangJin Han[1] · Jeong Hwan Chun[2] · Chan Hun Kim[2] · Do Heui Kim[1]

Received: 16 May 2024 / Revised: 2 July 2024 / Accepted: 3 July 2024 / Published online: 10 July 2024

Abstract

Activities and structures of metal oxide catalysts significantly rely on the synthesis procedures and conditions. In this study, a novel solvent-free mechanochemical method was employed to prepare catalysts for the ammoxidation of propylene. Multicomponent oxide catalysts containing bismuth, iron, cobalt, and molybdenum were successfully synthesized using a ball mill mixer and zirconia jars without the use of nitric acid. The mechanochemically synthesized catalysts exhibited higher catalytic performance than traditional catalysts prepared by coprecipitation (CP) and rotary evaporation (RE) methods in propylene ammoxidation. The synergistic effect of the mechanochemical method was investigated using various analyses, such as inductively coupled plasma atomic emission spectroscopy (ICP-AES), X-ray diffraction (XRD), scanning electron microscopy, energy-dispersive X-ray spectroscopy (EDS), Raman spectroscopy, and X-ray photoelectron spectroscopy (XPS). ICP-AES analysis revealed that the ball-mill-based catalysts contained metal elements in designated amounts more accurately than those prepared by the CP or RE methods. Propylene ammoxidation reactions with ball-milled catalysts showed a synergistic effect and improved acrylonitrile yield, especially at a 50:50 wt% ratio of $Bi_2Mo_3O_{12}$ to $Fe_{0.36}Co_{0.64}MoO_4$. Comprehensive analyses, including XRD, SEM–EDS, Raman spectroscopy, and XPS, support the conclusion that the improved performance of the mechanochemically synthesized catalysts can be attributed to the increased interaction between different phases prepared under mechanical forces, leading to a favorable change in the oxidation state of iron.

Keywords Propylene ammoxidation · Acrylonitrile production · Bismuth–iron–cobalt molybdate · Ball milling · Physical mixing

Introduction

The production of acrylonitrile (AN) by propylene ammoxidation is one of the largest and most commercially significant applications of metal oxide catalysts [1], constituting a global market exceeding ten billion USD. Initially commercialized by the Standard Oil Company of Ohio (SOHIO), the propylene ammoxidation process, also known as the SOHIO process, has its roots in research dating back to the 1950s and was first industrialized in the 1960s. [2, 3]. Over time, the SOHIO process has evolved into sophisticated multi-element metal oxide catalyst systems, incorporating an increasing number of metallic elements to improve efficiency and yield. The latest commercialized catalysts contain at least seven metallic elements, often as many as ten. Companies that have contributed to the commercialization and advancement of the SOHIO process include SOHIO [4], Asahi Kasei [5, 6], Mitsubishi Rayon [7], and INEOS [8]. AN, as a fundamental organic compound, serves as a monomer to produce valuable chemicals, such as acrylic fibers and engineering plastics. To produce AN, α-phase bismuth molybdenum-based metal oxides are well-known catalysts because of their outstanding activity and stability for multifunctional selective oxidation [9–11] in the catalysis field. However, the quest for a more efficient and eco-friendly approach for developing bismuth–molybdenum-based catalysts remains a persistent challenge.

✉ Do Heui Kim
dohkim@snu.ac.kr

[1] School of Chemical and Biological Engineering, Institute of Chemical Processes, Seoul National University, 1 Gwanak-ro, Gwanak-gu, Seoul 08826, South Korea

[2] R&D Center, Chemical Division, Hanwha Solutions, 76, Gajeong-ro, Yuseong-gu, Daejeon 34128, South Korea

One way to synthesize metal oxide catalysts is a chemical approach in which multiple metal precursors are dissolved in an acidic solvent in the preparation of catalysts. Licht et al. reported a coprecipitation method to investigate the mechanism of propylene ammoxidation catalysts [12], and House et al. proposed an evaporating-to-dryness method to control the metal ratios within the catalysts precisely [13]. Although these conventional methods can be used to synthesize high-quality metal oxide catalysts, they involve the use of nitric acid as a solvent, which can cause severe damage to the environment and biota. In addition, the coprecipitation method is prone to errors in the metal ratio owing to the difference in solubility between the metal elements depending on the pH conditions. In the evaporation method, the pH of the acid solution changes during the drying process, which can lead to problems such as the catalyst initially obtained from the wall of the flask being different from that later obtained from the bottom of the flask.

Several studies have reported the effective synthesis of various catalysts, including bulk metals, single-metal oxides, multi-metal mixed oxides, supported metals, and bimetallic alloy nanoparticles, using mechanochemical methods [14]. Among them, the α-bismuth molybdate catalyst system is known to possess a scheelite ($CaWO_4$) structure [15]. Mechanochemical synthesis of catalysts with similar scheelite structure or molybdate components has been reported for various applications such as photocatalysis e.g., ($BiVO_4$ [16–18], $BaMoO_4$ [19, 20], $ZnO/\alpha Fe_2O_3$ [21], $Ca_{12}Al_{14}O_{33}$ [22]), methanol oxidation to formaldehyde ($Fe_2(MoO_4)_3$ [23]), and oxidative dehydrogenation of ethanol ($Fe_2(MoO_4)_3$ reactions. However, no mechanochemical synthesis of bismuth–molybdenum-based multi-metal catalysts has been reported for propylene ammoxidation yet. In this research, we propose a new mechanochemical approach to synthesize bismuth–molybdenum-based metal oxide catalysts using a ball mill. Preparing multi-metal oxide catalysts using the ball milling method could eliminate the need for harmful acidic solvents [23]. The ball-mill-synthesized catalysts exhibited excellent performance in propylene ammoxidation and maintained a more stable structure than conventionally synthesized catalysts. Thus, the mechanochemical approach has proven to be practical in catalysis.

Experimental Section

Catalyst Preparation

A series of multi-metal molybdate catalysts were prepared using ball milling equipment, as shown in Fig. 1. Bismuth molybdate, a one-pot ball milling (BM) catalyst, was synthesized using a mechanochemical method. To achieve the Bi:Mo molar ratio of 2:3, specific proportions of bismuth nitrate pentahydrate ($Bi(NO_3)_3{\cdot}5H_2O$) and ammonium heptamolybdate tetrahydrate ($(NH_4)_5Mo_7O_{24}{\cdot}4H_2O$) were weighed and added to a 25 mL zirconium oxide jar. A 15 mm zirconium oxide ball was placed in the jar, then ball-milled at a frequency of 20 Hz for 30 min using a Retsch MM400 mixer mill. The resulting material was dried overnight and calcined at 530 °C for 5 h in the air to obtain the catalyst. The prepared catalyst was designated as $Bi_2Mo_3O_{12}$ one-pot BM. Similarly, an iron–cobalt molybdate one-pot ball milling (BM) catalyst was also synthesized to meet the Fe:Co:Mo molar ratio of 0.36:0.64:1.00. Specific proportions of iron nitrate nonahydrate ($Fe(NO_3)_3{\cdot}9H_2O$), cobalt nitrate hexahydrate ($Co(NO_3)_3{\cdot}6H_2O$) and ammonium heptamolybdate tetrahydrate ($(NH_4)_5Mo_7O_{24}{\cdot}4H_2O$) were weighed and added to a 25 mL zirconium oxide jar. A 15 mm zirconium oxide ball was placed in the jar which was then ball-milled at a frequency of 20 Hz for 30 min using a Retsch MM400 mixer mill. The resulting material was dried overnight and

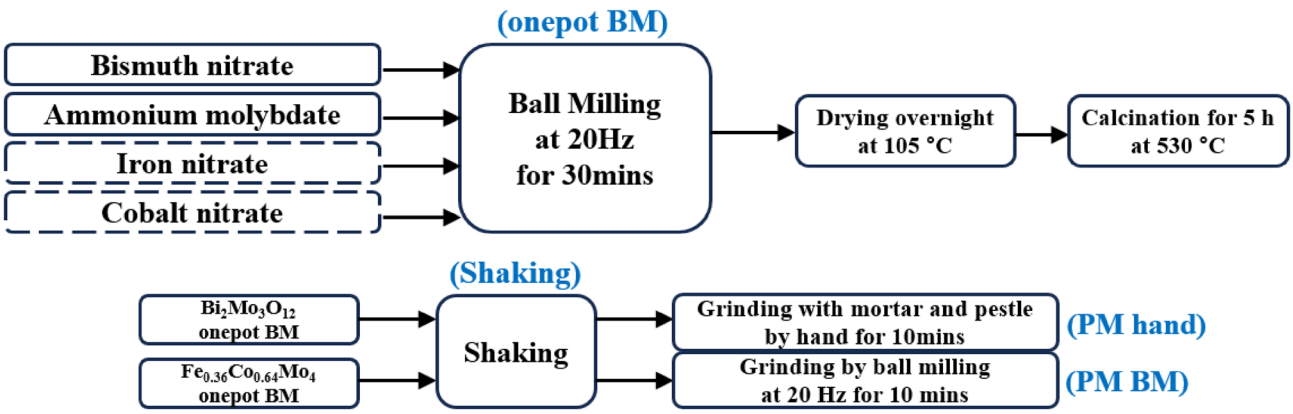

Fig. 1 Preparation procedures of one-pot ball milling (BM), shaking, physically mixed by hand (PM hand) and physically mixed by ball milling (PM BM) methods

then calcined at 530 °C for 5 h in the air. The catalyst was designated as $Fe_{0.36}Co_{0.36}MoO_4$ one-pot BM.

The shaking catalyst was prepared by shaking the $Bi_2Mo_3O_{12}$ one-pot BM catalyst and $Fe_{0.36}Co_{0.36}MoO_4$ one-pot BM without grinding. Subsequently, the first physically mixed catalyst was prepared by grinding and shaking the catalyst using an aluminum oxide mortar and pestle for 10 min. The catalyst was designated as PM hand and physically mixed manually. The second physically mixed catalyst was prepared by ball milling the shaking catalyst at a frequency of 20 Hz for 30 min. The catalyst was designated as PM BM and physically mixed by ball milling. The mixing ratios were designated according to the name of the catalyst. For example, a 50:50 PM hand catalyst was physically mixed with a hand catalyst in the ratio of 50 wt% $Bi_2Mo_3O_{12}$ one-pot BM and 50 wt% $Fe_{0.36}Co_{0.36}MoO_4$ one-pot BM.

A multi-metal one-pot catalyst was synthesized using a mechanochemical method. Specific proportions of metal precursors were weighed and added to a 25 mL zirconium oxide jar. A 15 mm zirconium oxide ball was placed in the jar, and the ball was milled at a frequency of 20 Hz for 30 min using an MM400 mixer mill. The resulting material was dried overnight and calcined at 530 °C for 5 h in the air to obtain the catalyst. This prepared catalyst was designated as a 50:50 one-pot BM.

Multi-metal molybdate catalysts have also been synthesized using conventional methods, such as coprecipitation (CP) and rotary evaporation (RE). Conventional synthetic methods are shown in Fig. 2.

To prepare the catalysts using the coprecipitation method, specific proportions of the metal precursors were weighed and added to deionized water. A small volume of nitric acid was then added to the solution, and the mixture was stirred using a magnetic bar and an agitator until it became transparent. The pH of the solution was adjusted using a pH meter, and ammonia solution was gradually added to the acidic solution until the desired pH was reached. The precipitated material was filtered using a vacuum filtration apparatus, dried overnight, and calcined at 530 °C for 5 h in the air to prepare the catalyst. The prepared catalysts were designated as CP pH x ($x = 1$, 4, 7, and 10).

To prepare the catalysts using the rotary evaporation method, specific proportions of the metal precursors were weighed and added to deionized water. A small volume of nitric acid was added to the solution and stirred using a magnetic bar and an agitator until the solution became transparent. The solution was heated to 80 °C, and the pressure dropped below 0.3 bar. The material was dried overnight and calcined at 530 °C for 5 h in air to obtain the catalyst. The prepared catalyst is referred to as RE.

Characterization

Inductively coupled plasma atomic emission spectroscopy (ICP-AES) was conducted using an Optima 8300 (PerkinElmer) instrument with an SCD detector. X-ray powder diffraction (XRD) patterns were obtained using a SmartLab (Rigaku) instrument with a 3 kW Cu target X-ray generator (40 kV, 40 mA). X-ray photoelectron spectroscopy (XPS), also known as electron spectroscopy for chemical analysis (ESCA), was performed using an AXIS Supra (Kratos) instrument with a monochromatic Al X-ray gun. Schottky field emission scanning electron microscopy (FE-SEM) and energy-dispersive X-ray spectroscopy (EDS) were performed using a JSM-7800F Prime (JEOL). Raman spectroscopy was performed using a DXR2xi (Thermo Fisher Scientific) with a 532 nm laser and an electron-multiplying charge-coupled detector (EMCCD).

Propylene Ammoxidation

The synthesized catalysts were tested in the propylene ammoxidation process using a continuous-flow fixed-bed reactor. The catalyst (0.5 g or 1.0 g) was loaded into a quartz reactor along with glass beads weighing twice the amount of the catalyst to prevent overheating from the highly exothermic reaction. The catalyst was preheated to 400 °C in a flow of nitrogen (20 mL/min) to eliminate residual water for 30 min and then heated to 430 °C in the flow of reactants (C_3H_6:NH_3: Air = 1:1.2:9.5), internal standard (Ne) and carrier gas (N_2). The total gas flow rate was maintained at 20 mL/min (SATP conditions). Reactions were performed at 430 °C for at least 6 h under atmospheric pressure. The products were analyzed using a gas chromatograph (ChroZen, YOUNGIN Chromass) equipped with a flame ionization detector (FID) and thermal conductivity detectors (TCD).

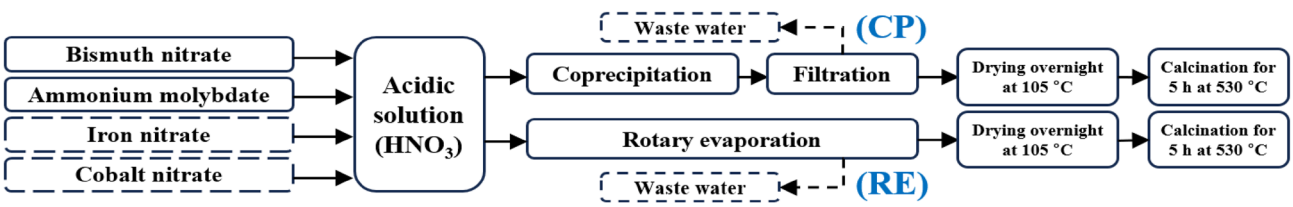

Fig. 2 Preparation procedures of coprecipitation (CP) and rotary evaporation (RE) methods

Molecular sieve 13X, Porapak N, and HP PLOT-Q columns were used for gas chromatography analysis. Propylene conversion, product selectivities, and acrylonitrile yield were calculated using the following equations: The flow rates were calibrated using an inert internal standard gas (Ne).

$$\text{Propylene conversion} = \frac{F_{\text{propylene,in}} - F_{\text{propylene,out}}}{F_{\text{propylene,in}}} \times 100, \quad (1)$$

$$S_i\,(\%) = \frac{F_i}{F_{\text{propylene,in}} - F_{\text{propylene,out}}} \times \frac{(\text{number of carbon atoms in } i)}{(\text{number of carbon atoms in propylene})} \times 100, \quad (2)$$

$$\text{AN yield}\,(\%) = \{\text{Propylene conversion}\,(\%)\} \times \left\{S_{\text{AN}}(\%)\right\} \div 100, \quad (3)$$

F_i flow rate of i, S_i selectivity of i.

Results and Discussion

Acrylonitrile Production by the Ammoxidation of Propylene

To successfully achieve the multifunctionality required in partial oxidation reactions, metal oxide catalysts must sequentially and seamlessly perform a complex process consisting of H-abstraction, O or N insertion, reduction of oxygen gas to lattice oxygen, lattice oxygen transfer, and reoxidation of H-abstraction sites [12, 24, 25]. There are various reports in the literature that utilize physical mixing [26–28]. By determining the optimal conditions for physical mixing, we can obtain the catalysts that outperform each catalyst alone. Physical mixing was performed to confirm the synergistic effect in the propylene ammoxidation reaction. The α-$Bi_2Mo_3O_{12}$ phase, known as the most effective catalyst for propylene amination reactions [29–31], was selected as phase 1. Furthermore, the propylene ammoxidation reaction follows the Mars–van Krevelen mechanism [32] in association with the lattice oxygen ions [33] in the metal oxide catalyst. Therefore, molybdates composed of Fe and Co, the transition metal species known to enhance the catalyst activity by improving redox performance through the lattice oxygen transfer [31, 34–38], were selected as phase 2.

Figure 3a shows propylene conversion, oxygen conversion, and AN yield. Figure 3b shows the selectivities of the products, which are acrylonitrile (AN), acrolein (ACR), acetonitrile (ACT), hydrogen cyanide (HCN), carbon monoxide (CO) and carbon dioxide (CO_2).

The activities of the PM BM catalysts with different mixing ratios ranging from 0:100 to 100:0 wt% were tested. Since the $Bi_2Mo_3O_{12}$ catalyst was selected as phase 1 and $Fe_{0.36}Co_{0.64}MoO_4$ as phase 2, the 0:100 ratio corresponds to 100 wt% $Fe_{0.36}Co_{0.64}MoO_4$ catalyst (pure phase 2), and the 100:0 ratio corresponds to 100 wt% $Bi_2Mo_3O_{12}$ catalyst (pure phase 1). When the $Fe_{0.36}Co_{0.64}MoO_4$ catalyst was physically mixed with the $Bi_2Mo_3O_{12}$ catalyst and then used in propylene ammoxidation, the conversion of propylene and the selectivity for AN increased compared to when each catalyst was used individually. Therefore, the physical mixing technique was empirically confirmed to induce synergistic interactions between the metal oxide phases.

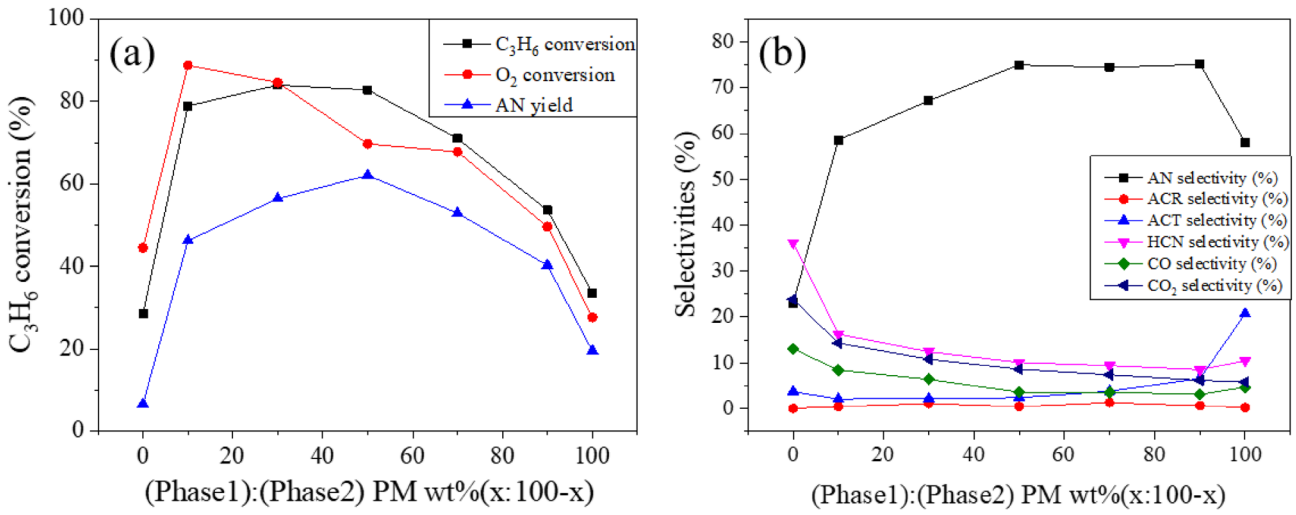

Fig. 3 (**a**) Conversions and yields with varying mixing ratio of PM BM catalysts. (**b**) Products' selectivities of PM BM catalysts ($x=0$: pure $Fe_{0.36}Co_{0.64}MoO_4$, $x=100$: pure $Bi_2Mo_3O_{12}$). *Catalysts loading: 1.0 g

The reaction activity of the physically mixed catalysts varied depending on the physical mixing ratio. Upon physical mixing, the propylene conversion ranged from 79 to 84% at 10:90, 30:70, and 50:50 wt% ratios. At higher percentages of $Bi_2Mo_3O_{12}$ catalyst, which are 70:30 and 90:10 wt% ratios, the propylene conversion decreased rapidly, while the AN selectivity remained high at approximately 75%. Therefore, it can be inferred that the production and supply of lattice oxygen are enhanced when the proportion of phase 2 increases. This is also confirmed by the activity results, which show that a higher proportion of phase 2 increases the conversion. This is at the expense of the selectivity for other oxides and partial oxides, especially CO, CO_2, and HCN. In addition, the change in the ratio revealed that the 50:50 ratio was the most optimal, with the highest AN yield as both the AN selectivity and propylene conversion remained high.

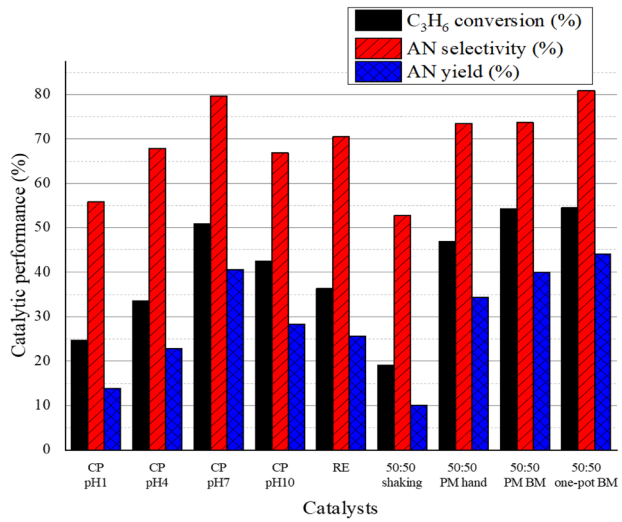

Fig. 4 Propylene conversions, AN selectivities and AN yields of 50:50 catalysts with different synthesis methods. *Catalysts loading: 0.5 g

As the reaction progressed, the catalyst performance increased, and the O_2 conversion reached 100%, reaching the detection limit. Instead of altering the O_2 ratio condition, further reaction experiments were conducted by reducing the contact time as well as reducing the catalyst loading from 1.0 g to 0.5 g while maintaining a uniform gas composition. The ratio of phase 1 to phase 2 was fixed at a 50:50 mass ratio, and the phases were prepared in several ways by changing the synthesis method. The reaction results for the catalysts prepared by various methods, such as CP under different pH conditions, RE, shaking, PM hand, PM BM, and one-pot BM, are summarized in Fig. 4.

Comparing the activity of the 50:50 PM and BM method with the same ratio preparation method in Figs. 3 and 4, the propylene conversion decreased significantly from 82.8 to 54.3% as the catalyst amount decreased from 1.0 to 0.5 g, while the AN selectivity remained almost unchanged from decreasing slightly from 75.0 to 74.3%. Therefore, reducing the contact time by adjusting the catalyst amount only affected the conversion rate and did not significantly affect AN selectivity, which was the main goal of this study within this contact time range.

As shown in Fig. 4, the best-performing catalyst was the 50:50 one-pot BM, followed by CP at pH 7. However, for the CP synthesis method, the decrease in catalyst performance with the change in pH was large, and the loss of metal elements was high as shown in Table 1. The RE method had a relatively high AN selectivity of 70.5%, although the AN yield was low because of the low propylene conversion rate compared to other catalysts, such as PM hand, PM BM, and one-pot BM. The lowest-performing catalyst was obtained with the 50:50 shaking, presumably because no external force was applied after shaking the catalysts. In contrast to the PM and one-pot BM catalysts, no direct interaction was observed between phases 1 and phase 2 in a 50:50 shaking catalyst. Despite the high temperature of about 430 °C, required for the propylene ammoxidation reaction, the 50:50 shaking catalyst did not exhibit any synergistic effect when

Table 1 Catalysts' compositions measured by ICP-AES

Catalysts	Fe atom ratio (STANDARD)	Bi atom ratio	Co atom ratio	Mo atom ratio
Designated ratio	2.50	3.37	4.45	12.00
CP pH1	2.50	4.10	0.02	12.91
CP pH4	2.50	3.41	0.72	9.67
CP pH7	2.50	3.23	3.97	6.23
CP pH10	2.50	2.56	0.68	1.26
RE	2.50	3.06	4.21	10.26
50:50 shaking	2.50	3.63	4.69	11.95
50:50 PM hand	2.50	3.41	4.60	11.61
50:50 PM BM	2.50	3.36	4.54	11.37
50:50 one-pot BM	2.50	3.14	4.28	11.00

the catalysts were simply shaken together at that temperature, resulting in a low conversion of 19% and AN selectivity of 52.7%. When phase 1 and phase 2 were physically mixed by hand (PM hand) in a 50:50 ratio, the propylene conversion increased significantly to 46.8% and the AN selectivity to 73.5% compared to the 50:50 shaking. When the PM method was performed using a ball mill instead of hands, the AN selectivity was nearly identical at 73.7%, whereas the propylene conversion increased slightly to 54.3%. For the one-pot BM catalyst, the propylene conversion was approximately the same as PM BM at 54.5%, whereas the AN selectivity increased significantly to 80.9%, resulting in the highest AN yield.

ICP Analysis of the Catalysts

Inductively coupled plasma atomic emission spectroscopy was performed to determine whether the metal species were precisely introduced into the prepared catalysts as intended. Table 1 summarizes the metal ratios in the catalysts. Iron was used as the standard for calculation to compare the metal species ratios.

All catalysts listed in Table 1 were prepared with the expectation that they would have an identical 50:50 phase ratio, which corresponds to a Fe:Bi:Co:Mo ratio of 2.50:3.37:4.45:12.00. For the CP catalysts, large amounts of Co were lost at pH1, pH4, pH10. At pH7, the Co content remained relatively constant although the Mo content was significantly lower than the specified ratio. The RE catalyst retained the metal species relatively well compared to the CP catalyst, although it did not retain the metal species as effectively as the ball-mill-based prepared catalyst. Conversely, the ball-mill-based prepared catalysts, including 50:50 shaking, PM hand, PM BM, and one-pot BM, retained the metal species much better, with minimal loss. Overall, ball-mill-based catalysts retained metal species much better than those prepared with RE.

Crystalline Structures of the Calcined Catalysts

XRD analysis was performed to investigate the crystalline structures of the metal oxide catalysts. XRD patterns were obtained and identified using a crystal information file (. cif) from the Crystallography Open Database (COD) [39]. The chemical formulas and the COD ID are listed in Table 2.

Figure 5 shows the XRD patterns of the CP pH1, pH4, pH7, pH10, and RE catalysts. Each catalyst exhibits its own pattern, composed of mixed metal oxide phases. The CP pH1 and pH4 catalysts were mainly composed of $Bi_2Mo_3O_{12}$ and $Fe_2Mo_3O_{12}$ phases. The CP pH 7 catalyst was mainly composed of $Fe_{0.3}Co_{0.7}MoO_4$ and $Bi_3FeMo_2O_{12}$ phases. CP pH10 catalyst was mainly composed of $BiMoO_6$, the γ-phase of bismuth molybdate, and did not show any sign of Fe or Co-related pattern. The RE catalyst exhibited four phases: $Bi_2Mo_3O_{12}$, $Fe_2Mo_3O_{12}$, $Fe_{0.3}Co_{0.7}MoO_4$, and $Bi_3FeMo_2O_{12}$. The results showed that the multimetallic complex oxide catalyst system can be represented by a combination of several phases, including $Bi_2Mo_3O_{12}$, $Fe_{0.3}Co_{0.7}MoO_4$, $Fe_2Mo_3O_{12}$, and $Bi_3FeMo_2O_{12}$.

Table 2 Chemical formulas and COD ID of the molybdate-based mixed oxides in XRD patterns

Chemical formula	COD ID	References
$Fe_2Mo_3O_{12}$	1524203	Chen [40]
Bi_2MoO_6	1537010	Zemann [41]
$Fe_{0.3}Co_{0.7}MoO_4$	2088874	Ehrenberg et al. [42]
$Bi_2Mo_3O_{12}$	7223785	Zhang et al. [43]
$Bi_3FeMo_2O_{12}$	7232465	Li et al. [44]

Figure 6 shows the XRD patterns of $Bi_2Mo_3O_{12}$, $Fe_{0.36}Co_{0.64}MoO_4$, and the 50:50 mixed catalysts. $Bi_2Mo_3O_{12}$ catalyst showed the same pattern as the theoretical calculations and reported data [45, 46]. $Fe_{0.36}Co_{0.64}MoO_4$ catalyst showed almost an identical pattern to the theoretical calculation result for $Fe_{0.3}Co_{0.7}MoO_4$ with a small addition of the $Fe_2Mo_3O_{12}$ pattern. Four 50:50 mixed catalysts showed almost the same pattern as that of the RE catalyst. Although the types of phases in the 50:50 catalysts are the same, their proportions differ slightly. The main difference in the pattern is approximately 28.6°.

To analyze the XRD patterns in more detail, Rietveld refinement or its extensions, such as Rietveld texture analysis (RITA) and Rietveld stress texture analysis (RISTA) techniques, were used [47, 48]. The phase quantification results of the 50:50 catalysts from in-depth analysis using RITA/RISTA techniques are shown in Table 3. The analyses were performed by material analysis using diffraction (MAUD) software [49] and structures with COD IDs, as shown in Table 2. The analysis showed that among the catalysts prepared using the ball mill, the catalysts with higher AN selectivity had a higher proportion of $Bi_3FeMo_2O_{12}$ phase, a single phase between Bi-Fe-Mo. $Bi_3FeMo_2O_{12}$ is known to form as a single phase upon the introduction of iron into the scheelite structure of α-$Bi_2Mo_3O_{12}$ [50]. $Bi_3FeMo_2O_{12}$ can promote the regeneration of depleted surface oxygens during the reoxidation cycle [31] and has been reported to exhibit similar activity to Bi–Mo–O phase for selective (amm)oxidation [51]. Grasselli, Burrington, and Brazdil have previously reported in mechanistic studies that $Bi_3FeMo_2O_{12}$ shows the same or similar mechanism as bismuth molybdate [52]. In multicomponent bismuth molybdates system with a common formula of $M_a^{2+}M_b^{3+}Bi_xMo_yO_z$, there are also papers showing a similar mechanism where bismuth activates propene and Mo inserts N or O into the activated allylic intermediate [53]. In these earlier studies, $Bi_3FeMo_2O_{12}$ showed lower

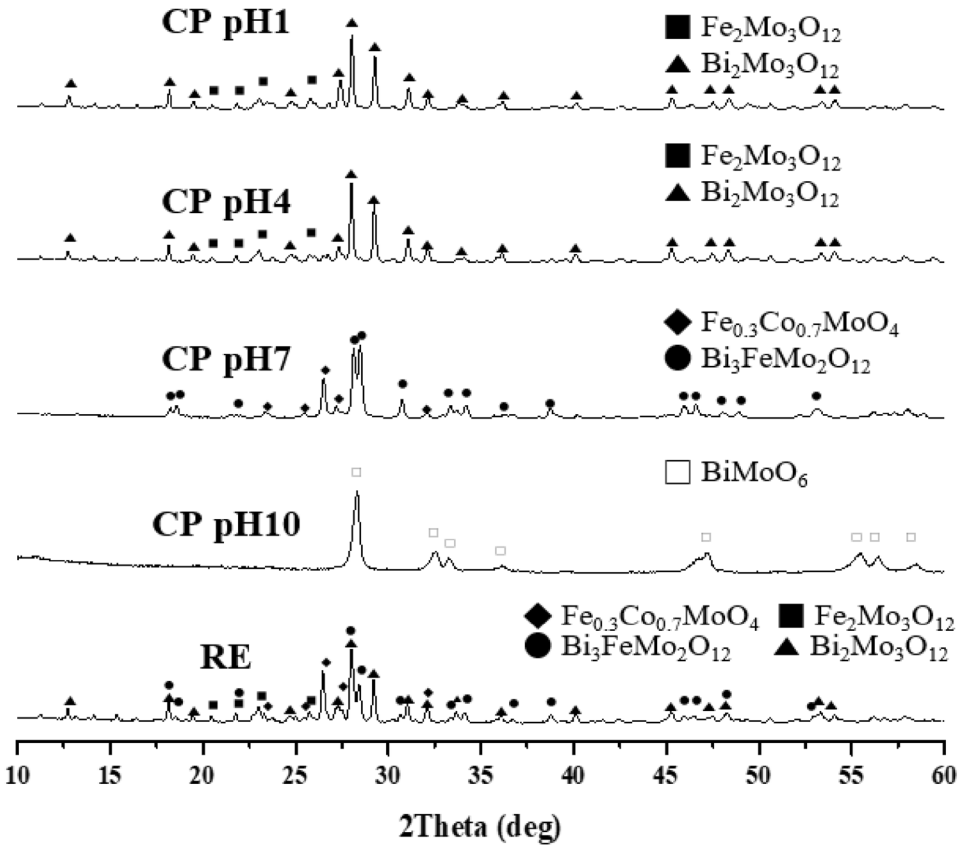

Fig. 5 Powder XRD patterns of CP prepared with different pH conditions and RE catalysts

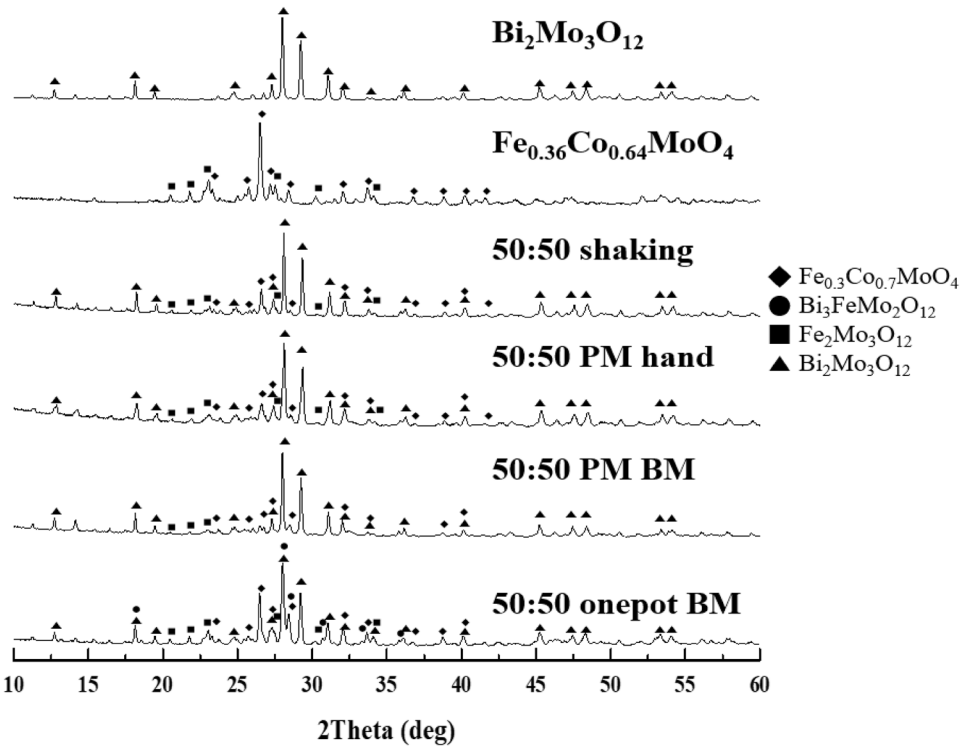

Fig. 6 Powder XRD patterns of $Bi_2Mo_3O_{12}$, $Fe_{0.36}Co_{0.64}MoO_4$ and 50:50 mixed catalysts

Table 3 Phase quantification results using Rietveld refinement of mixed catalysts

Sample	$Fe_2Mo_3O_{12}$ (wt%)	$Fe_{0.3}Co_{0.7}MoO_4$ (wt%)	$Bi_2Mo_3O_{12}$ (wt%)	$Bi_3FeMo_2O_{12}$ (wt%)	Total sum (wt%)
50:50 shaking	13.7	26.1	60.2	0.0	100.0
50:50 PM hand	12.5	24.3	61.3	1.9	100.0
50:50 PM BM	8.4	18.2	68.1	5.3	100.0
50:50 one-pot BM	19.3	31.9	35.2	13.6	100.0

activity than bismuth molybdate because $Bi_3FeMo_2O_{12}$ was the only phase used in the catalytic reaction. However, our findings in this work suggest that $Bi_3FeMo_2O_{12}$ has a positive synergistic effect when physically mixed with other phases. Moreover, it can be concluded that the increased interaction between phase 1 and phase 2 due to the application of external forces is a major factor in the improvement of the catalyst performance.

Further Characterizations of the Catalysts Synthesized by Ball Milling Method

Figure S1 (Online Resource 1) shows the scanning electron images of the ball-milled catalysts. Fig. S2 (Online Resource 1) shows a more detailed electron micrograph and EDS images of the 50:50 shaking catalyst. In the 50:50 shaking catalyst, in which no external force is applied, the metal elements are located on specific particles. For instance, Bi atoms are located on the $Bi_2Mo_3O_{12}$ particles but not on the $Fe_{0.36}Co_{0.64}MoO_4$ particles. In contrast, in the PM and one-pot BM catalysts, the metal elements are well dispersed and mixed on the same particle.

Figure S3 (Online Resource 1) shows the Raman spectra of ball-milled catalysts. Raman spectra show that the $Bi_2Mo_3O_{12}$ phase and $Fe_{0.36}Co_{0.64}MoO_4$ phase

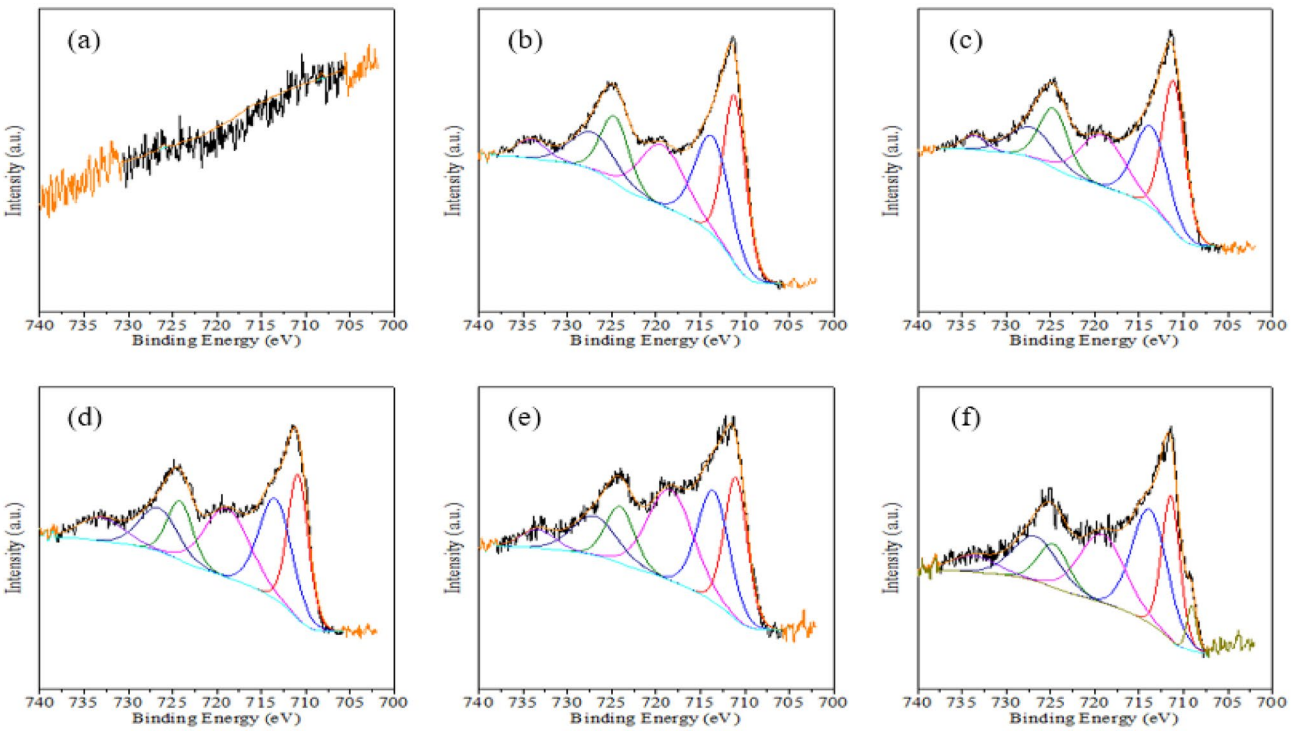

Fig. 7 XPS spectra of Fe 2p regions of catalysts; (**a**) $Bi_2Mo_3O_{12}$, (**b**) $Fe_2Mo_3O_{12}$, (**c**) 50:50 shaking, (**d**) 50:50 PM hand, (**e**) 50:50 PM BM and (**f**) 50:50 one-pot BM

Table 4 Oxidation state ratio of Fe from 2p region of XPS analysis

Chemical formula	Fe^{3+}/Fe^{2+} ratio
$Fe_{0.36}Co_{0.64}MoO_4$	0.91
50:50 shaking	0.79
50:50 PM hand	1.09
50:50 PM BM	1.12
50:50 one-pot BM	1.53

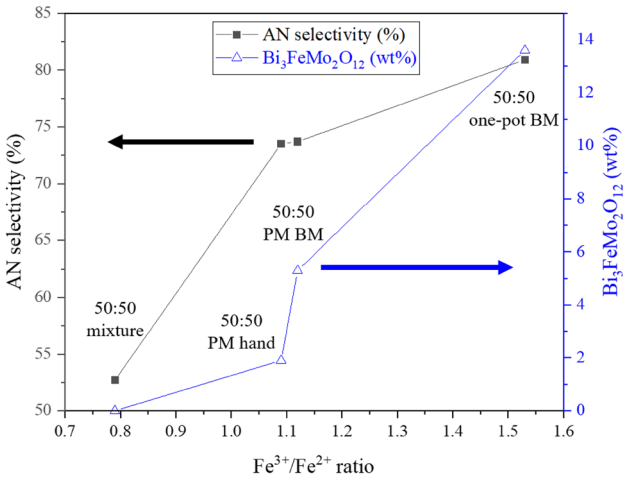

Fig. 8 Changes in AN selectivity and $Bi_3FeMo_2O_{12}$ weight ratio of catalysts plotted as a function of Fe^{3+}/Fe^{2+} ratio

are successfully incorporated into the 50:50 mixed catalysts. In 50:50 mixed catalysts, peaks at 75, 118, 195, 368, 814, and 900 cm^{-1} clearly show the trace of $Bi_2Mo_3O_{12}$ phase, and peaks around 777 and 935 cm^{-1} show $Fe_{0.36}Co_{0.64}MoO_4$ phase.

XPS analysis was also conducted to investigate the atomic states of the metal components on the surfaces of the 50:50 mixed catalysts. Figure 7 shows the XPS measurements of the 2p region of Fe, which plays a vital role in the inter-element interactions described in Fig. 6 and Table 3. The binding energy was calibrated using the C 1s peak (284.8 eV [54]) for all the spectra. Table 4 lists the ratio of Fe +3 to +2 oxidation states, calculated from the XPS 2p region. For the case of the $Bi_2Mo_3O_{12}$ catalyst, no Fe-related signal was measured. For the $Fe_{0.36}Co_{0.64}MoO_4$ catalyst, the ratio of Fe 3+ to 2+ oxidation states was 0.91. For the 50:50 shaking catalyst, introducing the $Bi_2Mo_3O_{12}$ catalyst reduced this value, but not quantitatively, by exactly half. The physically mixed catalysts showed an increase in the 3+ oxidation state compared to $Fe_{0.36}Co_{0.64}MoO_4$. Although PM BM had a slightly higher ratio of Fe3+ to 2+ oxidation states, PM hand, and PM BM had almost similar values with ratios of 1.09 and 1.12, respectively. In the one-pot BM catalyst, the ratio was 1.53, which is an apparent increase in the Fe^{3+} oxidation state ratio compared to previous catalysts. Therefore, it can be inferred from the XPS measurements that the change in the oxidation state of Fe has a positive effect on the AN selectivity.

Combined with the previous XRD patterns, it is evident that not only the AN selectivity but also the $Bi_3FeMo_2O_{12}$ phase ratio correlates with the Fe 2p oxidation state in the 50:50 ratio catalysts. Figure 8 shows the AN selectivities (Fig. 4) and $Bi_3FeMo_2O_{12}$ phase ratios (Table 3) as functions of the Fe oxidation state ratio (Table 4) for the catalysts prepared by ball milling. For the 50:50 PM hand catalyst, which had more interactions between phases than the 50:50 shaking catalyst, the $Bi_3FeMo_2O_{12}$ ratio increased from 0.0 to 1.9%, and the AN selectivity increased from 52.7 to 73.5%. In the 50:50 PM BM catalyst, the $Bi_3FeMo_2O_{12}$ ratio increased to 5.3%, and the AN selectivity increased to 73.7%. Finally, the 50:50 one-pot BM catalyst exhibited the highest value of $Bi_3FeMo_2O_{12}$ ratio of 13.6% and AN selectivity of 80.9%. Therefore, we confirmed that the increase in the Fe^{3+} oxidation state measured by XPS and the increase in the Bi–Fe–Mo interaction phase ratio measured by XRD had a positive synergistic effect on the AN selectivity of the catalyst.

Consequently, both the physical mixing and ball milling methods can be effectively used for the preparation of multicomponent metal oxide catalyst systems. Compared to traditional synthesis methods that promote metal element or ion exchange in aqueous solutions or require high-temperature or high-pressure conditions, mechanochemical synthesis methods are economical and environmentally friendly. In conventional multicomponent metal oxide synthesis methods, large amounts of nitric acid are required to mix metal precursors, such as Bi, Fe, Co, and Mo. In comparison, mechanochemical synthesis does not require harmful nitric acid and consumes less energy by stirring or rotating instead of heating. However, controlling the particle size of catalysts prepared by mechanochemical methods and exploring the mechanism of chemical changes caused by physical collisions between particles remain major challenges.

Conclusion

The ICP-AES analysis results indicate that the ball-mill-based catalysts are more effective in retaining metal elements than those prepared by the CP and RE methods. The ball-milled catalysts were then tested in propylene ammoxidation reactions. The physical mixing of $Bi_2Mo_3O_{12}$ with $Fe_{0.36}Co_{0.64}MoO_4$ resulted in a synergistic effect owing to interactions between the phases. While simple shaking in a 50:50 ratio showed no synergistic effect, catalysts that were physically mixed or prepared in one pot by ball milling

exhibited significant improvement in performance. Each catalyst exhibited distinct XRD patterns, revealing compositions, such as $Bi_2Mo_3O_{12}$, $Fe_{0.3}Co_{0.7}MoO_4$, $Fe_2Mo_3O_{12}$, and $Bi_3FeMo_2O_{12}$. Furthermore, Rietveld refinement and texture techniques indicated that catalysts with higher acrylonitrile selectivity had more of the $Bi_3FeMo_2O_{12}$ phase, suggesting enhanced catalyst performance through increased interactions between different phases under external forces. SEM–EDS analysis showed that the metal elements were located on specific particles in the 50:50 shaking catalyst, whereas in the PM and one-pot BM catalysts, the metal elements were uniformly dispersed and mixed. Raman spectroscopy confirmed that the two phases were mixed in an oxidized state in the mixed catalyst. X-ray photoelectron spectroscopy (XPS) analysis was employed to assess the atomic states of the metal components on the surfaces of the 50:50 mixed catalysts, focusing on the Fe 2p region. The XPS results indicated that the mechanochemical method led to an increase in the ratio of the 3+ to 2+ oxidation states of Fe, suggesting a positive correlation between the change in the Fe oxidation state and increased acrylonitrile selectivity.

Supplementary Information The online version contains supplementary material available at https://doi.org/10.1007/s11814-024-00218-x.

Acknowledgements This research was supported and funded by Hanwha Solutions Chemical Division.

Data availability Data will be made available on request.

References

1. R.K. Grasselli, Fundamental principles of selective heterogeneous oxidation catalysis. Top. Catal. **21**(1/3), 79–88 (2002). https://doi.org/10.1023/a:1020556131984
2. J.D.J. Idol, Process for the manufacture of acrylonitrile, Patent publication No. US 2904580 (1959)
3. J.L. Callahan, R.W. Foreman, F. Veatsch, Process for the oxidation of olefins, Patent publcation No. US 2941007 (1960)
4. C. Paparizos, M.J. Seely, M.S. Friedrich, D.D. Suresh, Improved catalyst for the manufacture of acrylonitrile, Patent publication No. WO 02/13963 (2002)
5. A. Fukuzawa, M. Kaneta, Catalyst for fluidized bed ammoxidation reaction, and method for producing acrylonitrile, Patent publication No. WO 2017/130909 (2018)
6. J. Yoshida and T. Yamaguchi, Oxide catalyst and method for producing the same, and methods for producing unsaturated aldehyde, diolefin, and unsaturated nitrile (2016)
7. K. Nishida, M. Yanagita, T. Karasuda, H. Watanabe, Method for producing acrylonitrile, Patent publication No. WO 2013/129385 (2013)
8. J. F. Brazdil, S. S.-Y. Lin, Ammoxidation catalysts containing samarium, Patent publication No. WO 2017/069995 (2017)
9. J.F. Brazdil, A critical perspective on the design and development of metal oxide catalysts for selective propylene ammoxidation and oxidation. Appl. Catal. A Gen. **543**(June), 225–233 (2017). https://doi.org/10.1016/j.apcata.2017.06.022
10. J.C. Védrine, Heterogeneous partial (Amm)oxidation and oxidative dehydrogenation catalysis on mixed metal oxides. Catalysts (2016). https://doi.org/10.3390/catal6020022
11. R.K. Grasselli, Site isolation and phase cooperation: two important concepts in selective oxidation catalysis: a retrospective. Catal. Today **238**, 10–27 (2014). https://doi.org/10.1016/j.cattod.2014.05.036
12. R.B. Licht, D. Vogt, A.T. Bell, The mechanism and kinetics of propene ammoxidation over α-bismuth molybdate. J. Catal. **339**, 228–241 (2016). https://doi.org/10.1016/j.jcat.2016.04.012
13. M.P. House, A.F. Carley, R. Echeverria-Valda, M. Bowker, Effect of varying the cation ratio within iron molybdate catalysts for the selective oxidation of methanol. J. Phys. Chem. C **112**(11), 4333–4341 (2008). https://doi.org/10.1021/jp711251b
14. A.P. Amrute, J. De Bellis, M. Felderhoff, F. Schüth, Mechanochemical synthesis of catalytic materials. Chem. A Eur. J. **27**(23), 6819–6847 (2021). https://doi.org/10.1002/CHEM.202004583
15. J.F. Brazdil, Scheelite: a versatile structural template for selective alkene oxidation catalysts. Catal. Sci. Technol. **5**(7), 3452–3458 (2015). https://doi.org/10.1039/c5cy00387c
16. V.-I. Merupo, S. Velumani, K. Ordon, N. Errien, J. Szade, A.-H. Kassiba, Structural and optical characterization of ball-milled copper-doped bismuth vanadium oxide ($BiVO_4$). CrystEngComm **17**(17), 3366–3375 (2015)
17. S. Deka, M.B. Devi, M.R. Khan, Keerthana, A. Venimadhav, B. Choudhury, Piezo-photocatalytic and photocatalytic bismuth vanadate nanorods with antibacterial property. ACS Appl. Nano Mater. **5**(8), 10724–10734 (2022)
18. Q. Han, Advances in preparation methods of bismuth-based photocatalysts. Chem. Eng. J. **414**, 127877 (2021)
19. O.M. Baby, S. Balamurugan, S.A. Ashika, T.K.S. Fathima, Synthesis and characterization of high NIR reflecting eco-friendly $BaMoO_4$ pigments in scheelite family. Emerg. Mater. 1–13 (2022)
20. X. Xu, Y. Pan, Y. Zhong, L. Ge, Z. Shao, From scheelite $BaMoO_4$ to perovskite $BaMoO_3$: enhanced electrocatalysis toward the hydrogen evolution in alkaline media. Compos. Part B Eng. **198**, 108214 (2020)
21. A. Dehghan, A. Aliasghar, R. Rahmati, M. Delnavaz, H. Khoshvaght, Green synthesis of ZnO/αFe_2O_3 nano-photocatalyst for efficient removal of carbamate pesticides in wastewater: optimization, mineralization, and financial analysis. Korean J. Chem. Eng. **41**, 249–269 (2024). https://doi.org/10.1007/s11814-024-00073-w
22. J. Hye Park, M. Woo Hong, W. Oo, J. Joon Park, H. Ju Park, K. Bok Yi, Enhanced photocatalytic activity of TiO_2/$Ca_{12}Al_{14}O_{33}$ in NO removal. Korean J. Chem. Eng. **40**(12), 2906–2913 (2023). https://doi.org/10.1007/s11814-023-1485-0
23. L. Tao Kong et al., Green and rapid synthesis of iron molybdate catalyst by mechanochemistry and their catalytic performance for the oxidation of methanol to formaldehyde. Chem. Eng. J. **364**, 390–400 (2019). https://doi.org/10.1016/j.cej.2019.01.164
24. J.F. Brazdil, Designing multifunctionality into single phase and multiphase metal-oxide-selective propylene ammoxidation catalysts. Catalysts (2018). https://doi.org/10.3390/catal8030103
25. J.D. Burrington, C.T. Kartisek, R.K. Grasselli, Surface intermediates in selective propylene oxidation and ammoxidation over heterogeneous molybdate and antimonate catalysts. J. Catal. **87**(2), 363–380 (1984). https://doi.org/10.1016/0021-9517(84)90197-0
26. M.T. Le et al., Synergy effects of the mixture of bismuth molybdate catalysts with SnO_2/ZrO_2/MgO in selective propene oxidation and the connection between conductivity and catalytic activity. Ind. Eng. Chem. Res. **55**(17), 4846–4855 (2016). https://doi.org/10.1021/acs.iecr.6b00019
27. J.M.M. Millet, H. Ponceblanc, G. Coudurier, J.M. Herrmann, J.C. Vedrine, Study of multiphasic molybdate-based catalysts: II. Synergy effect between bismuth molybdates and mixed iron and

cobalt molybdates in mild oxidation of propene. J. Catal. **142**(2), 381–391 (1993)
28. I. Song et al., Simple physical mixing of zeolite prevents sulfur deactivation of vanadia catalysts for NO_x removal. Nat. Commun. **12**(1), 901 (2021)
29. M. Egashira, Phase diagram of the system Bi_2O_3-MoO_3. J. Catal. **58**(3), 409–418 (1979). https://doi.org/10.1016/0021-9517(79)90279-3
30. D. Carson, G. Coudurier, M. Forissier, J.C. Vedrine, A. Laarif, F. Theobald, Synergy effects in the catalytic properties of bismuth molybdates. J. Chem. Soc. Faraday Trans. 1 Phys. Chem. Condens. Phases **79**(8), 1921–1929 (1983)
31. J.F. Brazdil, D.D. Suresh, R.K. Grasselli, Redox kinetics of bismuth molybdate ammoxidation catalysts. J. Catal. **66**(2), 347–367 (1980)
32. P. Mars, D.W. van Krevelen, Oxidations carried out by means of vanadium oxide catalysts. Chem. Eng. Sci. **3**, 41–59 (1954). https://doi.org/10.1016/S0009-2509(54)80005-4
33. G.W. Keulks, L.D. Krenzke, T.M. Notermann, Selective oxidation of propylene, in *Advances in Catalysis*, vol. 27 (Elsevier, 1979), pp. 183–225
34. J. Engeldinger et al., Probing the structural changes and redox behavior of mixed molybdate catalysts under ammoxidation conditions: an operando raman spectroscopy study. ChemCatChem **8**(5), 976–983 (2016). https://doi.org/10.1002/cctc.201501276
35. X. Wu, G. Yu, X. Chen, Y. Wang, C. Liu, Reduction/reoxidation of a multicomponent molybdate catalyst for propylene ammoxidation. Thermochim. Acta **486**(1–2), 20–26 (2009)
36. B. Delmon, J. Haber, J.H. Block, Manual of methods and procedures for catalyst characterization (technical report). Pure Appl. Chem. **67**(8–9), 1257–1306 (1995). https://doi.org/10.1351/pac199567081257
37. J. Haber, Cobalt and other transition metal molybdate catalysts. J. Less Common Met. **36**(1–2), 277–287 (1974)
38. A. Ghalwadkar, B. Katryniok, S. Paul, A.S. Mamede, F. Dumeignil, Role of promoters on the acrolein ammoxidation performances of $BiMoO_x$. JAOCS J. Am. Oil Chem. Soc. **93**(3), 431–443 (2016). https://doi.org/10.1007/s11746-015-2785-2
39. S. Gražulis et al., Crystallography open database—an open-access collection of crystal structures. J. Appl. Crystallogr. **42**(4), 726–729 (2009)
40. H. Chen, The crystal structure and twinning behavior of ferric molybdate, $Fe_2(MoO_4)_3$. Mater. Res. Bull. **14**(12), 1583–1590 (1979)
41. J. Zemann, Die Kristallstruktur von Koechlinit, Bi_2MoO_6. Heidelberger Beiträge zur Mineral. und Petrogr. **5**, 139–145 (1956)
42. H. Ehrenberg, I. Svoboda, M. Wiesmann, H. Weitzel, A mixed transition metal molybdate, β-$(Co_{0.7}Fe_{0.3})MoO_4$. Acta Crystallogr. Sect. C Cryst. Struct. Commun. **55**(9), 1383–1384 (1999)
43. Y. Zhang et al., Effect of high bismuth deficiency on structure and oxide ion conductivity of a $Bi_{0.55}MoO_4$ single crystal. CrystEngComm **17**(45), 8746–8751 (2015)
44. C. Li et al., Bulk crystal growth and characterization of the bismuth ferrite-based material $Bi_3FeO_4(MoO_4)_2$. CrystEngComm **21**(15), 2508–2516 (2019)
45. R. Gruar, C.J. Tighe, L.M. Reilly, G. Sankar, J.A. Darr, Tunable and rapid crystallisation of phase pure Bi_2MoO_6 (koechlinite) and $Bi_2Mo_3O_{12}$ via continuous hydrothermal synthesis. Solid State Sci. **12**(9), 1683–1686 (2010). https://doi.org/10.1016/J.SOLIDSTATESCIENCES.2010.07.001
46. K. Aykan, Reduction of Bi_2O_3-MoO_3 catalyst during the ammoxidation of propylene in the absence of gaseous oxygen. J. Catal. **12**(3), 281–290 (1968)
47. H.R. Wenk, S. Matthies, L. Lutterotti, Texture analysis from diffraction spectra, in *Materials Science Forum*, Trans Tech Publ, pp. 473–480 (1994)
48. M. Ferrari, L. Lutterotti, Method for the simultaneous determination of anisotropic residual stresses and texture by x-ray diffraction. J. Appl. Phys. **76**(11), 7246–7255 (1994)
49. L. Lutterotti, S. Matthies, H. Wenk, MAUD: a friendly Java program for material analysis using diffraction. CPD Newsl. **21**, 14–15 (1999)
50. W. Jeitschko, A.W. Sleight, W.R. McClellan, J.F. Weiher, A comprehensive study of disordered and ordered scheelite-related $Bi_3(FeO_4)(MoO_4)_2$. Acta Crystallogr. Sect. B **32**(4), 1163–1170 (1976). https://doi.org/10.1107/S056774087600486X
51. W.J. Linn, A.W. Sleight, Oxidation of 1-butene over bismuth molybdates and bismuth iron molybdate. J. Catal. **41**(1), 134–139 (1976). https://doi.org/10.1016/0021-9517(76)90208-6
52. R.K. Grasselli, J.D. Burrington, J.F. Brazdil, Mechanistic features of selective oxidation and ammoxidation catalysis. Faraday Discuss. Chem. Soc. **72**, 203 (1981). https://doi.org/10.1039/dc9817200203
53. J.D. Burrington, C.T. Kartisek, R.K. Grasselli, Aspects of selective oxidation and ammoxidation mechanisms over bismuth molybdate catalysts *II. Allyl alcohol as a probe for the allylic intermediate. J. Catal. **63**(1), 235–254 (1980). https://doi.org/10.1016/0021-9517(80)90076-7
54. D. Fang, F. He, J. Xie, L. Xue, Calibration of binding energy positions with C1s for XPS results. J. Wuhan Univ. Technol. Sci. Ed. **35**, 711–718 (2020)